Journal of Dynamical Systems and Complexity (2026) vol.1(2): 37-48
eISSN: 3122-4326, DOI: 10.66131/JDSC12202637-48

Chaotic Time Series Analysis with the Wavelet Transform

L.J. Ontanon-Garcia[1], R. E. Lozoya Ponce [2], E. Jiménez-López[3*]*

[1]CARAO, UASLP, Salinas de Hidalgo, S.L.P, México.
[2]Tecnológico Nacional de México - Campus Chihuahua, Chihuahua 31200, México;
[3]Centro de Investigación y Estudios Avanzados de la Población, UAEMex, Toluca 50110, México.

Abstract

This work presents the numerical implementation and evaluation of a chaotic system that generates multiple attractors, and analyzes these attractors using time-series data via the wavelet transform. This technique enables the examination of time-frequency fluctuations at multiple resolutions, facilitating the identification of complex and transient patterns in chaotic behavior. A key characteristic of chaotic systems is their high sensitivity to initial conditions. black Visualizing chaotic dynamics through wavelet-based power time–scale (scalogram) representations facilitates an understanding of their evolution. Moreover, this approach enables the detection of transient patterns and significant changes in the time series, providing insight into transitions between chaotic states. The multi-resolution decomposition inherent to the wavelet transform also enhances the accuracy of predictive models for chaotic time series.

Keywords— Chaotic system, multiple attractors, wavelet transform, multi-resolution analysis.

1 Introduction

This work presents the numerical implementation and evaluation of a chaotic system that generates multiple scrolls, and analyzes them using time-series data and the wavelet transform. This technique enables the examination of time-frequency fluctuations at multiple resolutions, facilitating the identification of complex and transient patterns in chaotic time series. Wavelet transform analysis is based on multi-resolution decomposition, which breaks a signal into components at different scales and frequencies, enabling the exploration of both long-term and short-term dynamics [1].
Many natural phenomena and processes are inherently nonlinear. One particularly intriguing manifestation of nonlinearity is chaotic behavior. In the early 1960s, meteorologist Edward Lorenz attempted to extend weather forecasting beyond four or five days. To do so, he developed a simplified nonlinear model consisting of three equations with three independent variables, thereby reducing the vast number of variables typically involved in atmospheric modeling. This model provided only a qualitative description of the chaotic evolution of climate systems [2].
A key characteristic of chaotic systems is their extreme sensitivity to initial conditions—small variations at the start of a process can lead to vastly different outcomes. Although numerous systems exhibit chaotic behavior, particular interest lies in those whose responses oscillate chaotically. Examples include the Lorenz, Rössler, and Chua systems, which are frequently analyzed using numerical techniques [3].

Among the various mathematical tools available for analyzing signals generated by chaotic systems, the wavelet transform stands out for its ability to characterize time series in terms of energy distribution and to extract additional information from systems exhibiting multiple chaotic attractors. These analyses aim to identify patterns and transitions inherent to chaotic dynamics. Visualizing chaotic behavior using the wavelet transform produces representations akin to power spectrograms, aiding in the understanding of how such dynamics evolve across time and scale [4, 5, 6].

The wavelet transform offers a distinct advantage in analyzing chaotic time series due to its adaptability to non-stationary data. Since chaotic signals are inherently non-stationary, this technique is particularly well-suited for

*Corresponding author: ejimenezl@uaemex.mx
Received: September 19, 2025, **Published:** Jun 30, 2026
Edited by: E. Campos Cantón

their study. Additionally, it enables the identification of transient patterns and the detection of key events or signal changes, offering insight into transitions between different chaotic states [7].
Seminal treatments of wavelets for signal analysis can be found in Mallat (1999) [8], while several works specifically apply wavelet-based diagnostics to chaotic and hyperchaotic time series (Murguía & Campos-Cantón, 2006; Murguía et al., 2018 [9, 10]). These studies motivate our use of the wavelet variance and scalogram-type diagnostics to characterize scale-localized features of multi-scroll attractors. Another notable benefit of the wavelet transform is its ability to filter out noise, thereby facilitating the identification of underlying chaotic structures in a signal. By analyzing dynamics across multiple scales, it reveals features and patterns that would remain hidden with traditional Fourier-based methods [11, 12].

The wavelet transform has been successfully applied to analyze chaotic time series originating from numerical simulations, electronic circuits, and physical systems. Its multi-resolution decomposition also enhances the accuracy of predictive models. Furthermore, it has been used in biomedical contexts to analyze electroencephalographic (EEG) and electrocardiographic (ECG) signals, revealing chaotic or irregular behaviors [13].
This paper is organized as follows: Section 2 provides an overview of the discrete wavelet transform. Section 3 details the numerical implementation of a chaotic system capable of generating multiple scrolls. Section 4 presents the wavelet-based analysis applied to the resulting time series. Finally, Section 5 offers concluding remarks.

2 Wavelet Transform

The wavelet transform is an alternative and complementary mathematical technique to the Fourier transform [12, 14]. Its discrete version helps determine the energy distribution of coefficients, revealing information about the chaotic time series that generated them. The wavelet transform is particularly useful for analyzing dynamic signals originating from chaotic systems or oscillators [15].

First, the scaled–translated wavelet family is described by [8, 9, 10]:

$$\psi_{a,b}(t) = \frac{1}{\sqrt{a}}\,\psi\left(\frac{t-b}{a}\right), \qquad a > 0, b \in \mathbb{R}. \tag{1}$$

While the continuous wavelet transform is defined by equation (2).

$$W_f(a,b) = \frac{1}{\sqrt{a}}\int_{-\infty}^{\infty} f(t)\psi\left(\frac{t-b}{a}\right)dt. \tag{2}$$

Here, $\psi(t) \in L^2(\mathbb{R})$ may be real or complex-valued. The inner product in $L^2(\mathbb{R})$ is defined as $<f, \psi_{a,b}> := \int_{\infty}^{\infty} f(t)\overline{\psi_{a,b}(t)}dt$, where the overline denotes complex conjugation. This ensures that the continuous wavelet transform defines a proper Hilbert-space projection. $a \in \mathbb{R}^+$ ($a \neq 0$) is the scale or dilation parameter, and $b \in \mathbb{R}$ is the translation parameter.

The discrete wavelet transform involves defining a discrete grid for these parameters (a, b). For computational efficiency, they are discretized using a dyadic scheme, as shown in equation (3).

$$a = 2^{-j}; \quad b = k2^{-j} = ka; \tag{3}$$

where j and k are the dilation and translation indices, which are integers. The discrete form of the wavelet function is defined by equation (4).

$$\psi_{j,k}(t) = 2^{j/2}\psi(2^j t - k). \tag{4}$$

By substituting equation (1) into (2), the discrete wavelet transform can be expressed as in equation (5).

$$f_{j,k} = W_f(2^{-j}, k2^{-j}) = \int_{-\infty}^{\infty} f(t)\psi_{j,k}(t)dt. \tag{5}$$

The reconstruction of the time series from the coefficients $\psi_{j,k}$ yields the orthonormal basis shown in equation (6).

$$f(t) = \sum_{j=-\infty}^{\infty}\sum_{k=-\infty}^{\infty} f_{j,k}\psi_{j,k}(t) \tag{6}$$

Representing the time series using an orthonormal wavelet basis facilitates both analytical and computational processing. The contribution of the time series at a particular wavelet level j is given by equation (7).

$$f_j(t) = \sum_k f_{j,k}\psi_{j,k}(t) \tag{7}$$

Implementing the discrete wavelet transform numerically requires techniques such as multi-resolution analysis to derive the wavelet basis. This framework enables hierarchical decomposition of time series into sub-bands. Figure 1 illustrates the structure of multi-resolution analysis as a decomposition of vector space.

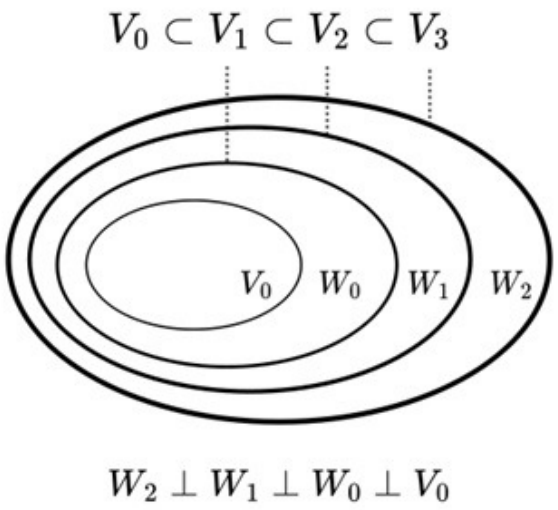

Figure 1: Multi-resolution analysis of the vector space using the scaling function $\varphi(t)$ and wavelet function $\psi(t)$.

In multi-resolution analysis, the wavelet function is associated with the scaling function $\varphi(t)$, which generates the approximation spaces V_j by integer shifts and dyadic dilations. Whereas ψ, generates the detail spaces $\{W_j\}$, which are orthonormal complements of V_j, satisfying the relation $V_{j+1} = V_j \oplus W_j$. Since $\varphi \in V_0 \subset V_1$ and $\psi \in W_0 \subset V_1$, the scaling function and wavelet satisfy equations (8) and (9). Therefore, Equation (4) defines the discrete wavelet basis functions $\psi_{j,k}$ used for the DWT expansion.

$$\varphi(t) = \sqrt{2}\sum_{k\in Z} h_k\varphi(2t-k), \tag{8}$$

$$\psi(t) = \sqrt{2}\sum_{k\in Z} g_k\varphi(2t-k). \tag{9}$$

Here, $g_k = (-1)^n h_{1-k}$. Based on multi-resolution analysis, the decomposition of a finite time series $f \in L^2(\mathbb{R})$ is shown in equation (10).

$$f(t) = \sum_{k=1}^{2^{j_0}} c_{j_0,k}\varphi_{j_0,k}(t) + \sum_{j=j_0}^{j-1}\sum_{k=1}^{2^j} f_{j,k}\psi_{j,k}(t) \tag{10}$$

The corresponding scale and wavelet coefficients are computed as shown in equations (11) and (12).

$$c_{j_0,k} = \int_{-\infty}^{\infty} f(t)\varphi_{j_0,k}(t)dt \tag{11}$$

$$f_{j,k} = \int_{-\infty}^{\infty} f(t)\psi_{k,j}(t)dt \tag{12}$$

In practice, for discrete signals, these coefficients are computed using the discrete wavelet transform (DWT) implemented via the Mallat filter-bank (pyramid) algorithm [16], which performs convolution with quadrature mirror filters followed by dyadic subsampling at each decomposition level.

Many physical signals exhibit scale invariance, meaning their structure remains consistent across scales. These include waveforms with fractal characteristics. In particular, an important class of statistically scale-invariant

functions is the family of $1/f$ random processes [17]. A signal $f(t)$ is considered statistically self-similar if it satisfies the scaling relationship in equation (13).

$$f(t) \cong a^{-H} f(at) \tag{13}$$

Where $a > 0$, and the equivalence symbol denotes that both signals have the same statistical properties. The time-scale structure of the wavelet transform makes it particularly effective for analyzing functions and distributions that exhibit self-similarity. If a signal $f(t)$ is self-similar, its wavelet transform will also exhibit self-similar properties. For such signals, the variance of the wavelet coefficients $f_{j,k}$ follows equation (14).

$$\text{var}(f_{j,k}) \approx (2^j)^{-\beta} \tag{14}$$

Here, $\beta = 2H + 1$, where H is the self-similarity parameter. The scaling law in (13) and the relation $\beta = 2H + 1$ follow from the wavelet variance scaling for self-similar processes; see Wornell & Oppenheim (1992) and Abry & Veitch (1998) [18, 19] for derivations connecting the Hurst exponent H with the spectral exponent β).

Beyond the spectral exponent β, the self-similarity parameter H is also connected to other scaling exponents commonly used in fractal analysis. In detrended fluctuation analysis (DFA), the fluctuation function scales as:

$$F(s) \sim s^{\alpha}, \tag{15}$$

where for monofractal processes $\alpha = H$. In multifractal DFA (MF-DFA), the generalized fluctuation functions obey

$$F_q(s) \sim s^{h(q)}, \tag{16}$$

where $h(2) = H$ for statistically self-similar signals. Thus, the exponent H represents a particular case within a broader class of scaling exponents that characterize long-range correlations and scale invariance.

The relationship in equation (14) helps characterize different types of time series. If the energy is evenly distributed across most levels, the time series behaves like noise. In contrast, if a few adjacent levels concentrate most of the energy, it indicates a dominant or carrier frequency. These characteristics can be observed by plotting the logarithm of the variance of wavelet coefficients against level j, as will be illustrated later in the text.

Remark (scale vs. frequency): In the wavelet transform, the dilation parameter a (scale) is inversely related to pseudo-frequency: roughly, $f \propto f_c/a$, where f_c is the wavelet's center frequency (dependent on the chosen mother wavelet). Thus, a small a (low scale) corresponds to high-frequency content and a large a to low-frequency content. The exact scale–frequency mapping depends on the mother wavelet. See Mallat (1999) [8].

3 Chaotic Attractor with Multiple Scrolls

This section provides a brief overview of the numerical implementation of a chaotic system capable of generating numerous scrolls for studying chaotic time series. Although structurally simple, these systems exhibit complex chaotic behavior that has attracted significant attention across mathematics, physics, and engineering [20, 21]. We consider a class of linear systems defined by equation (17).

$$\dot{x} = Ax + B \tag{17}$$

Here, $x = [x_1, x_2, x_3]^T \in \mathbb{R}^3$ is the state vector, $B = [\beta_1, \beta_2, \beta_3]^T \in \mathbb{R}^3$ is a constant vector, and $A = [\alpha_{ij}] \in \mathbb{R}^{3\times3}$ represents a linear operator. The system's equilibrium points are given by $x_0^* = -A^{-1}B$ [22, 23].

The system dynamics can be derived from the third-order linear differential equation $\dddot{x} + \alpha_{33}\ddot{x} + \alpha_{32}\dot{x} + \alpha_{31}x + \beta_3 = 0$, which corresponds to the state-space formulation in equation (17). The matrices A and B are defined as:

$$A = \begin{pmatrix} 0 & 1 & 0 \\ 0 & 0 & 1 \\ -\alpha_{31} & -\alpha_{32} & -\alpha_{33} \end{pmatrix}; \quad B = \begin{pmatrix} 0 \\ 0 \\ \beta_3 \end{pmatrix}, \tag{18}$$

where the parameters $\alpha_{31}, \alpha_{32}, \alpha_{33} \in \mathbb{R}$ are arbitrary scalars chosen to ensure that the system remains piecewise linear. Specifically, the trace condition $Tr(A) = \sum_{i=1}^{3} \lambda_i < 0$ must hold, and the characteristic polynomial $g(\lambda) = \lambda^3 + \alpha_{33}\lambda^2 + \alpha_{32}\lambda + \alpha_{31}$ should have one negative real eigenvalue and a complex pair with positive real part [24]. For this work, we use $\alpha_{31} = 1.5$, $\alpha_{32} = 1$, and $\alpha_{33} = 1$.

To produce multiple scrolls, we introduce a switching control signal β_3 that alternates between two values, S_1 and S_2, resulting in two distinct equilibrium points and generating a double-scroll attractor. By incorporating additional piecewise-linear segments into the switching function, we can extend this approach to generate chaotic attractors with multiple scrolls, with the number of scrolls determined by the number of switching regions. This control signal depends on a single state variable, typically x_1, and defines domain boundaries through hyperplanes aligned with a coordinate axis [22].

The control signal described by equation (19) generates a double-scroll chaotic attractor:

$$\beta_3 = \begin{cases} S_1 = 1.8, & \text{if } x_1 \geq 0.3; \\ S_2 = -0.9, & \text{otherwise.} \end{cases} \tag{19}$$

Using equations (17)–(19), the equilibrium points are calculated as $x_0^{*1} = (0.6, 0, 0)^T$ and $x_0^{*2} = (0, 0, 0)^T$.

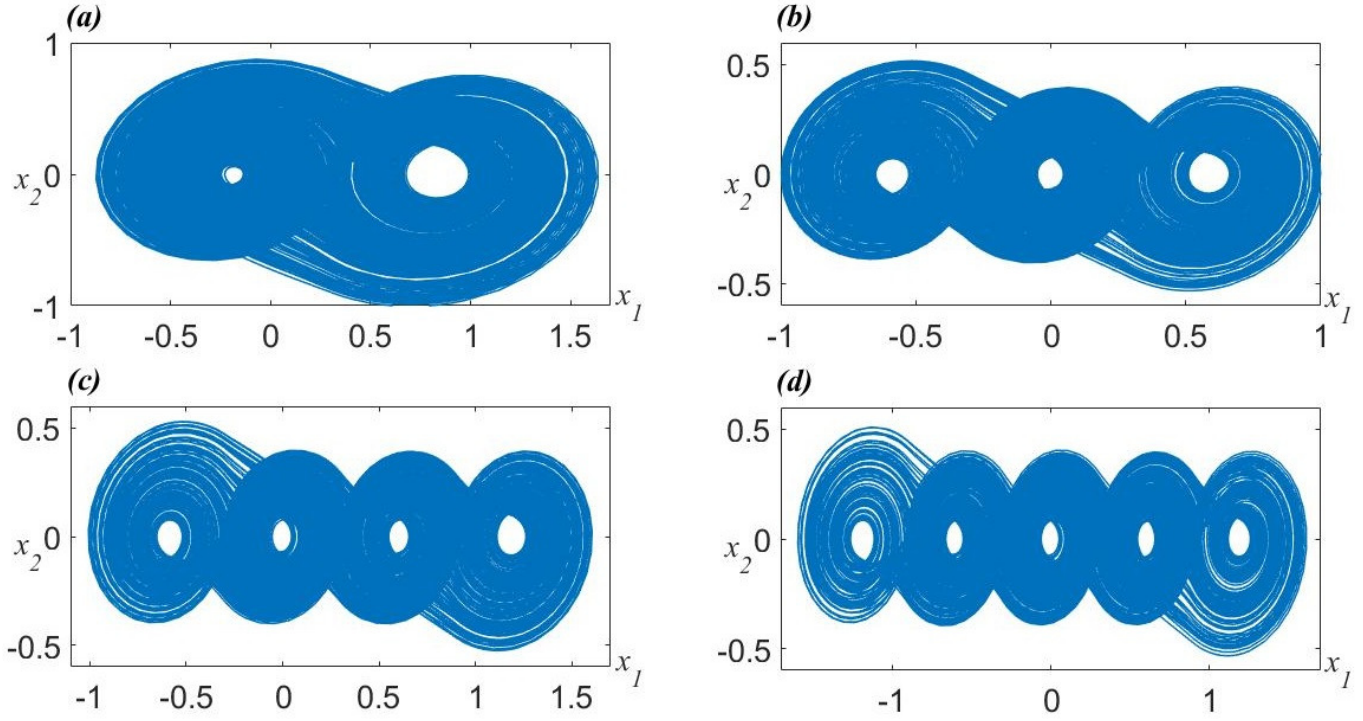

Figure 2: Multiple Scrolls.

Figure 2(a) shows the projection of the resulting two-scroll chaotic attractor on the (x_1, x_2) plane. By modifying the control signal, we generate a three-scroll chaotic attractor, as defined in equation (20):

$$\beta_3 = \begin{cases} 0.9, & \text{if } x_1 \geq 0.3; \\ 0, & \text{if } -0.3 < x_1 < 0.3; \\ -0.9, & \text{if } x_1 \leq -0.3. \end{cases} \tag{20}$$

Note that the equilibrium point x_0^{*3} is the negative of x_0^{*1}, resulting in a symmetric attractor structure, as illustrated in Figure 2(b). The projection in the (x_1, x_2) plane clearly reveals the presence of three scrolls.

To generate attractors with four or five scrolls, we continue using equations (17) and (18), introducing additional switching boundaries. The control signal for the four-scroll system is given by equation (21), while equation (22) defines the signal for five scrolls:

$$\beta_3 = \begin{cases} 1.8, & \text{if } x_1 \geq 0.9; \\ 0.9, & \text{if } 0.3 < x_1 < 0.9; \\ 0, & \text{if } -0.3 < x_1 < 0.3; \\ -0.9, & \text{if } x_1 \leq -0.3. \end{cases} \tag{21}$$

$$\beta_3 = \begin{cases} 1.8, & \text{if } x_1 \geq 0.9; \\ 0.9, & \text{if } 0.3 < x_1 < 0.9; \\ 0, & \text{if } -0.3 < x_1 < 0.3; \\ -0.9, & \text{if } -0.9 < x_1 \leq -0.3; \\ -1.8, & \text{if } x_1 \leq -0.9. \end{cases} \tag{22}$$

The equilibrium points $x_0^{*4} = (1.2, 0, 0)^T$ and $x_0^{*5} = (-1.2, 0, 0)^T$ are added to the existing set of fixed points. Figure 2(c) displays the projection of the four-scroll attractor, while Figure 2(d) shows the projection for five scrolls. All the time series were generated by numerically integrating Eq. (17) with Eq. (18) and the switching laws from Eqs. (19)-(22) using a fixed-step fourth-order Runge–Kutta integrator (RK4). We used an integration step of 1.0×10^{-3} s, and initial condition $x(0) = (0.1,\ 0,\ 0)^T$ unless otherwise stated. The first $1,024$ samples were discarded to remove transient behavior before analysis.

4 Analysis of Chaotic Time Series

We analyze the chaotic time series generated by the system capable of producing multiple scrolls, as shown in Figure 2. This analysis is conducted using the wavelet transform, applied to the time series derived from the system described above. The interpretation is based on the energy distribution of the wavelet coefficients at different resolution levels. The objective is to determine whether the energy distribution across these levels reveals additional insights into the structure of chaotic time series, as illustrated in Figure 3.

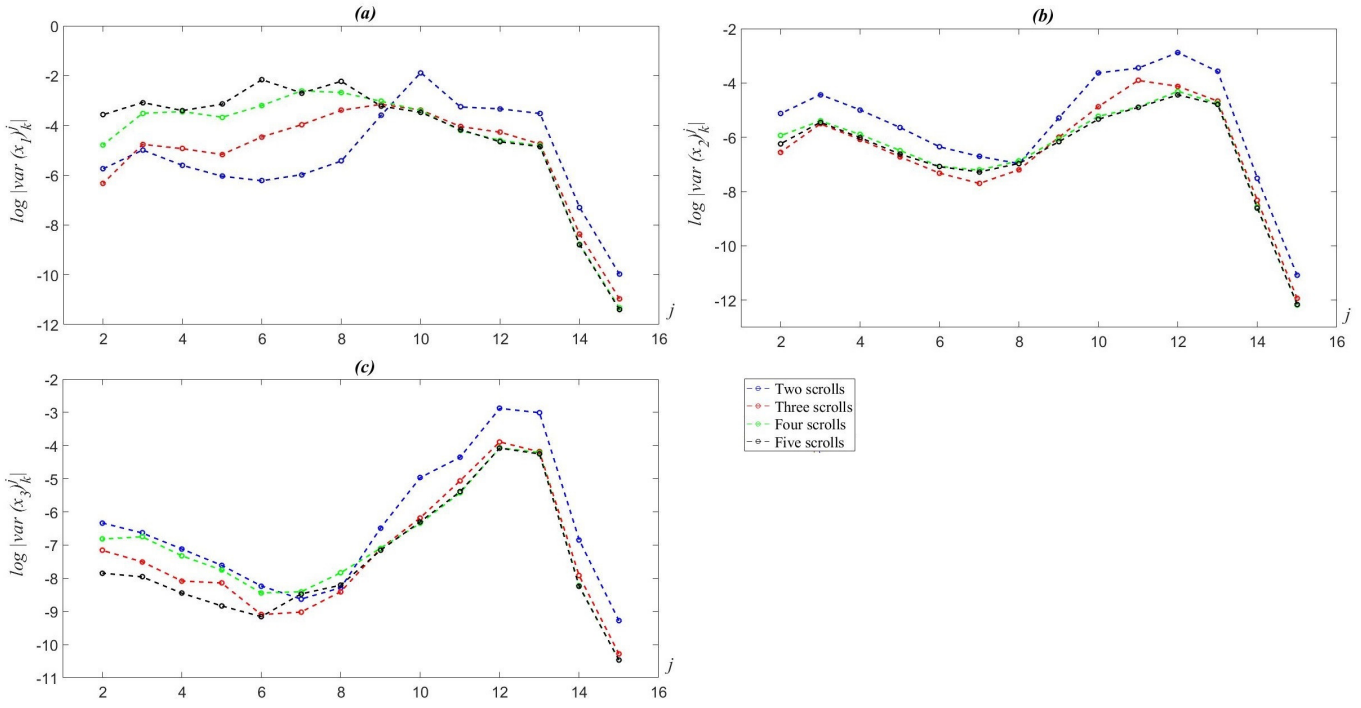

Figure 3: Analysis of time series generated with multiple scrolls using the wavelet transform.

Previous studies have examined different types of time series, identifying properties that depend on the nature of the underlying signal. Time series with chaotic dynamics generated through simulations (for instance [**Murgia2018**, 9]) or electronic circuits form the basis for the current investigation. In general, analyzing a chaotic time series enables the identification of specific features or patterns in the data. The following observations clarify how such behavior can be characterized:

1. A localized peak in the semi-log variance indicates a concentrated carrier-like component (see Murguía & Campos-Cantón, 2006 [9]).
2. A near-zero slope corresponds to broadband, noise-like energy distribution (Wornell & Oppenheim, 1992 [18]).

3. A negative slope indicates scale-invariance/fractal-like dynamics; the slope is related to the spectral exponent $\beta = 2H + 1$ (Wornell & Oppenheim, 1992 [18]).

These behaviors can be interpreted through the logarithm of the variance as a function of resolution levels, based on equation (14), which involves the coefficients $f_{j,k}$, the resolution levels j, and the self-similarity exponent β. This section aims to characterize the behavior of chaotic time series, particularly those with multi-scroll dynamics described in earlier sections.

Figure 3(a) presents the wavelet analysis of the state variable x_1 for systems with varying numbers of scrolls. For the two-scroll system (blue dotted line), the energy is concentrated at level $j = 10$, indicating a dominant frequency component. As the number of scrolls increases, the energy distribution becomes more uniform across levels. Figure 3(b) shows the analysis for state x_2, where the two-scroll system exhibits significant energy at level $j = 12$, suggesting distinct dynamics compared to higher-scroll systems. Figure 3(c) shows similar results for state x_3, where the two-scroll system again displays dominant energy at levels $j = 12$ and $j = 13$, indicating that combining these levels results in a more accurate signal reconstruction.

It is also evident from Figure 3 that as the number of scrolls increases, especially in state x_1—the coordinate that defines the multi-scroll behavior—the energy distribution changes. Initially, the graph shows a positive slope at lower-resolution levels, transitioning to a negative slope at higher-resolution levels. This shift reflects a transformation toward fractal behavior in the time series, particularly in state x_1.

We now analyze in detail the wavelet transform applied to the time series produced by the three-scroll chaotic system shown in Figure 2(b), with the results presented in Figure 4.

Figure 4(a) displays the time series of state x_1 from the three-scroll system (see Figure 2(b)). The series consists of $32,768$ points, corresponding to a maximum decomposition level of $m = \log_2(32768) = 15$. Figure 4(b) presents the logarithmic variance of the wavelet coefficients as a function of level j, using the Daubechies $db8$ wavelet. Which was selected for its balance between compact support and sufficient vanishing moments, providing good localization of both transient and low-frequency components in chaotic signals [9, 25]. In addition, the db8 was selected due to its eight vanishing moments and compact support, which provide an appropriate compromise between time localization and frequency selectivity. Since wavelet-based scaling estimation requires the number of vanishing moments to exceed the signal's regularity exponent, db8 provides sufficient smoothness for robust characterization of fractal-like behavior in the analyzed time series [26, 27, 28]. Up to level $j = 9$, the energy distribution resembles that of white noise, with a near-zero slope and relatively high energy. From level $j = 10$ onward, the variance decreases progressively, indicating fractal-like behavior.

A partial reconstruction of x_1 using coefficients from levels $j = 8$ to $j = 11$ is shown in Figure 4(c). The corresponding reconstruction error is displayed in Figure 4(d), where an oscillating error of approximately 25% amplitude suggests that energy is spread across more levels, and that additional levels should be included to achieve higher accuracy.

Figure 5 presents the same type of analysis for state x_2. Figure 5(a) shows the numerical data, while Figure 5(b) plots the logarithmic variance of the wavelet coefficients. A pronounced peak is observed at level $j = 11$. Since levels $j = 12$ and $j = 13$ also show high energy, all three levels were used for reconstruction, shown in Figure 5(c). The result confirms a high energy concentration, indicative of a carrier frequency. The reconstruction error is shown in Figure 5(d).

Finally, Figure 6 presents the analysis of state x_3. The time series is shown in Figure 6(a), and the logarithmic variance of wavelet coefficients is displayed in Figure 6(b), revealing a dominant frequency component. Figure 6(c) shows the reconstruction using levels $j = 12$ and $j = 13$, which account for the highest energy. The reconstruction error, shown in Figure 6(d), confirms the adequacy of these two levels.

The link between a negative slope in the semi-log variance plot and fractal (self-similar) dynamics follows from the scaling law (13): for self-similar processes, the wavelet coefficient variance scales as $(2^j)^{-\beta}$, and $\beta > 0$ indicates scale-invariance with fractal properties [29, 18]. Practically, concentrated energy (localized peaks) is desirable for reconstruction and signal recovery tasks; by contrast, distributed/fractal energy profiles increase the difficulty of selective reconstruction and are potentially advantageous for masking/encryption. We emphasize that which behavior is 'desirable' depends on the application: (i) for trajectory reconstruction or reduced-order modeling, choose states/scales with localized energy; (ii) for secure communication, states with distributed energy across scales may

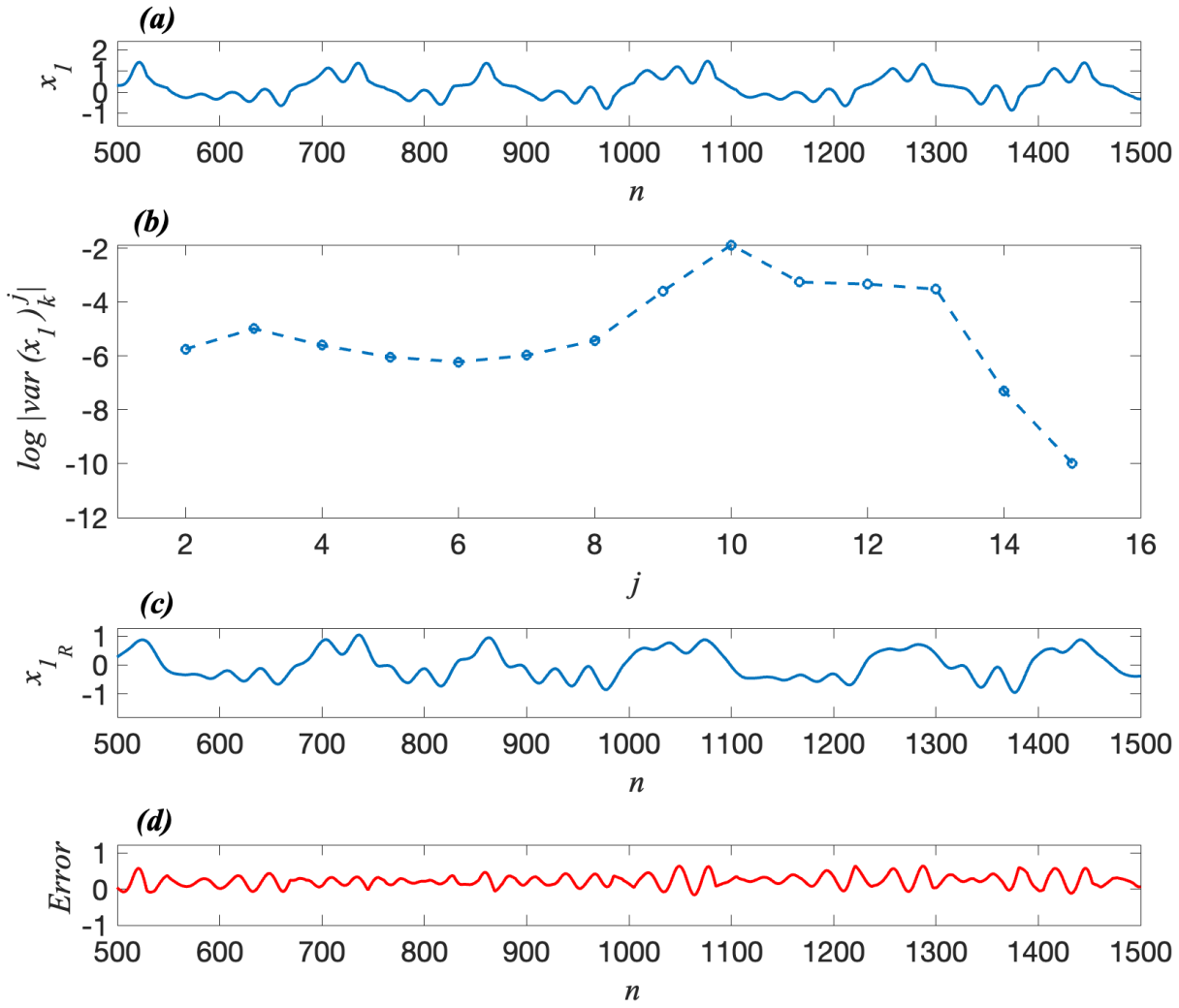

Figure 4: (a) Numerical data for state x_1; (b) logarithm of the variance of the wavelet coefficients; (c) reconstruction using four wavelet levels; (d) error between the original and reconstructed signal.

provide natural masking.

In summary, for the three-scroll system shown in Figure 2(b), reconstructing state x_1 requires at least four wavelet levels. State x_2 concentrates energy in three levels, while state x_3 shows strong energy in just two levels. As the number of scrolls increases beyond two ($n > 2$), the system exhibits similar behavior across all states. In such cases, the energy variance across levels exhibits a negative slope, characteristic of fractal behavior.

5 Conclusion

This work presented the numerical implementation of a chaotic system capable of generating multiple scrolls and its corresponding analysis using the wavelet transform. The objective was to identify characteristic features that could help determine the origin and nature of time series associated with chaotic attractors exhibiting multi-scroll behavior. The results confirm that the wavelet transform is a powerful mathematical tool for analyzing signals, particularly for capturing energy distributions across multiple resolution levels. By applying this transform to chaotic time series, we identified distinguishing features related to the structure and complexity of the underlying dynamics. The observed patterns were consistent across systems with chaotic behavior, providing a meaningful characterization of the attractors.

It was observed that as the number of scrolls increases, the energy distribution in state x_1—the state governing scroll generation in phase space—undergoes a clear transition. Specifically, the slope of the energy distribution in the

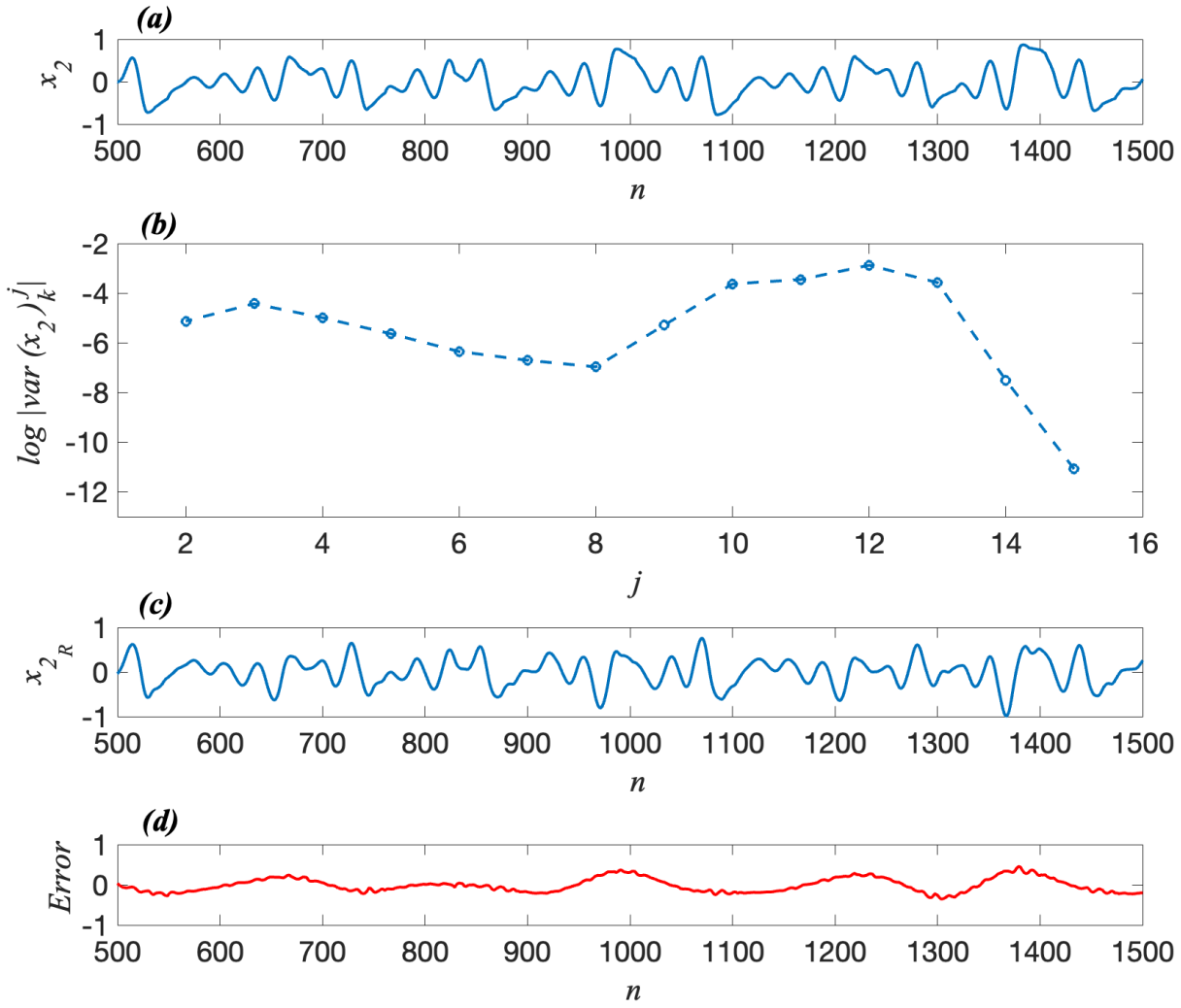

Figure 5: (a) Numerical data for state x_2; (b) logarithm of the variance of wavelet coefficients; (c) reconstruction using three wavelet levels; (d) error between the original and reconstructed signal.

semi-logarithmic variance plot shifts from slightly positive to negative, indicating the emergence of fractal behavior. In contrast, the energy distribution of states in which scroll generation is not dominant remains relatively stable.
States x_2 and x_3 exhibited similar behavior across different scroll configurations, characterized by two key components: a Gaussian-noise-like pattern and a carrier frequency. The noise-like behavior corresponds to a flat (zero-gradient) profile in the semi-logarithmic plot of wavelet coefficient variance. At the same time, the carrier frequency manifests as a localized energy peak over two or three consecutive resolution levels, followed by a negative slope indicative of fractal behavior.
For state x_1, a transition point at level $j = 8$ marks the shift from noise-like to fractal behavior. In states x_2 and x_3, energy is concentrated at specific levels, with reconstructions using just a few wavelet bands yielding a strong representation of the original signal—evidence of a dominant frequency component. This observation suggests that states x_2 and x_3 carry structural information that is relatively independent of system dynamics, unlike state x_1.
The presence of energy concentration in only a few levels for states x_2 and x_3 should not be surprising, as these states are not directly responsible for scroll generation. Their behavior makes them suitable candidates for signal recovery tasks. Through wavelet analysis, we can identify which states provide richer information content, thereby supporting selective signal reconstruction or masking strategies in chaotic systems.
Wavelet transforms have become increasingly popular in recent years for analyzing energy distributions across different resolution levels. They are used in various applications, including data compression, noise removal, biomedical signal analysis, frequency and time localization analysis, fractal and turbulence modeling, and communication

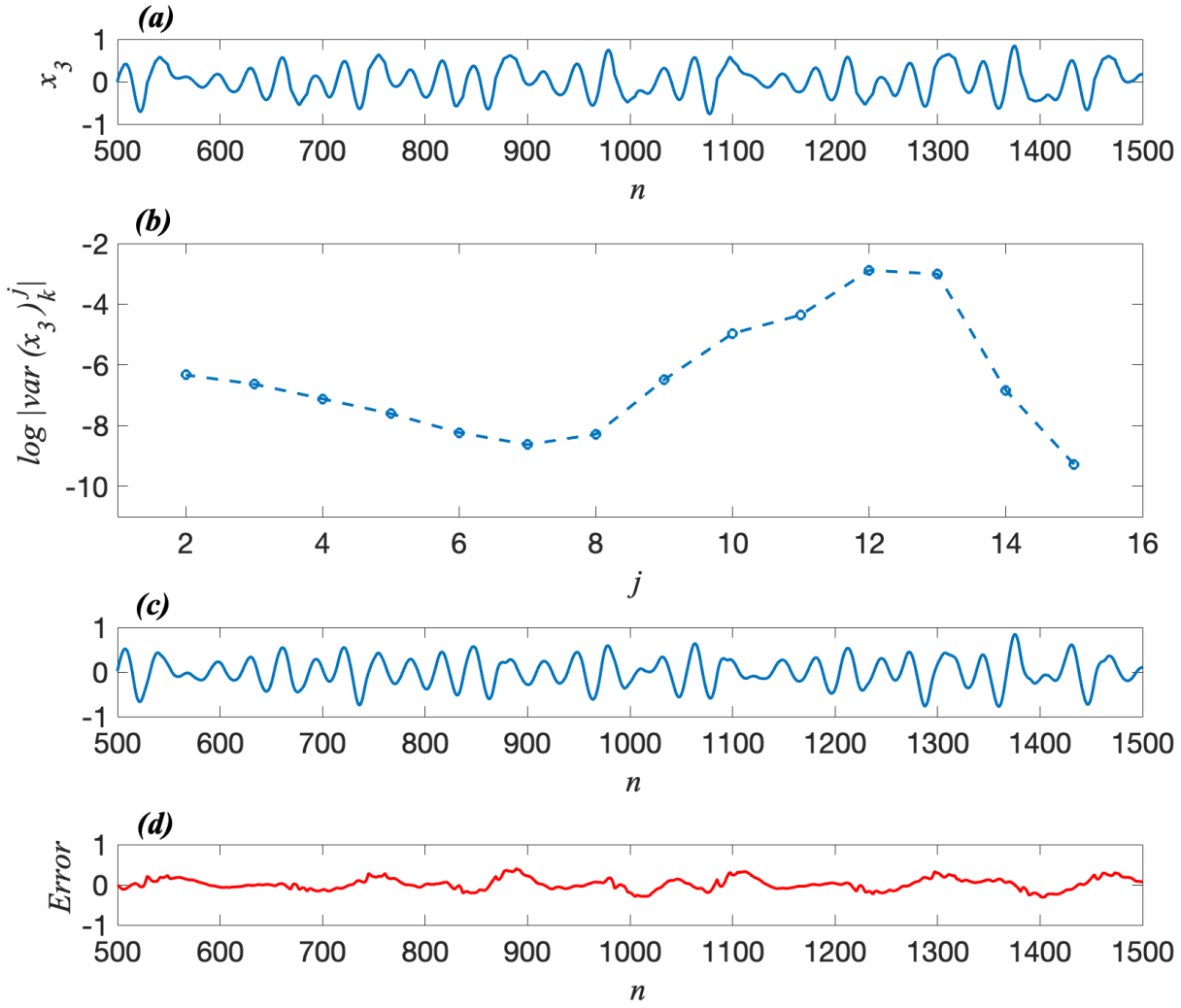

Figure 6: (a) Numerical data for state x_3; (b) logarithm of the variance of wavelet coefficients; (c) reconstruction using two wavelet levels; (d) error between the original and reconstructed signal.

systems, among many others. The key lies in matching the shape of the parent wavelet to the shape of the features being isolated in the time series (peaks, edges, regularity, etc.). Therefore, future work will review different wavelet functions and provide evidence to determine which is best suited for the analysis.

This study provides a strong foundation and motivation for continued research in both numerical simulation and experimental validation of multi-scroll chaotic systems. Beyond characterizing energy concentration in modulated states, this method can be extended to detect optimal states for information masking or encryption. Future work should investigate the effect of external noise on the system, particularly in practical implementations. Moreover, the potential of this system as a secure communication channel—by leveraging its natural masking properties—warrants integrating signal encryption schemes with wavelet-based analysis.

Additionally, the observed wavelet energy profiles suggest the design of intelligent classification or prediction algorithms based on resolution-level signatures. This could lead to applications in signal diagnostics, pattern recognition in nonlinear systems, or the identification of time-series anomalies using a compact and efficient set of features derived from wavelet coefficients.

Acknowledgments

L.J.O.G. Thanks to the Potosino Council of Science and Technology (COPOCYT) for the support in Trust project 23871 of the 2023-01 Call.

References

[1] W. Wu et al. "Unraveling Multi-Scale dynamics of estuarine wetland vegetation using the multi-resolution analysis wavelet transform and the Landsat time-series". In: *Ecological Indicators* 158 (2024), p. 111342. DOI: 10.1016/j.ecolind.2023.111342.

[2] C. Touzé, A. Vizzaccaro, and O. Thomas. "Model order reduction methods for geometrically nonlinear structures: a review of nonlinear techniques". In: *Nonlinear Dynamics* 105.2 (2021), pp. 1141–1190. DOI: 10.1007/s11071-021-06693-9.

[3] A. Mashuri et al. "Application of chaos theory in different fields–a literature review". In: *Journal of Science and Mathematics Letters* 12.1 (2024), pp. 92–101. DOI: 10.37134/jsml.vol12.1.11.2024.

[4] A. Szczęsna et al. "Chaotic biomedical time signal analysis via wavelet scattering transform". In: *Journal of Computational Science* 72 (2023), p. 102080. DOI: 10.1016/j.jocs.2023.102080.

[5] Z. Tian. "Analysis and research on chaotic dynamics behaviors of wind power time series at different time scales". In: *Journal of Ambient Intelligence and Humanized Computing* 14.2 (2023), pp. 897–921. DOI: 10.1007/s12652-021-03343-1.

[6] J. Hu et al. "Attractor memory for long-term time series forecasting: A chaos perspective". In: *arXiv preprint arXiv:2402.11463* (2024). DOI: 10.48550/arXiv.2402.11463.

[7] P. C. Li et al. "A novel model for chaotic complex time series with large of data forecasting". In: *Knowledge-Based Systems* 222 (2021), p. 107009. DOI: 10.1016/j.knosys.2021.107009.

[8] S. Mallat. *A Wavelet Tour of Signal Processing*. San Diego, CA: Academic Press, 1999.

[9] J. S. Murguía and E. Campos-Cantón. "Wavelet analysis of chaotic time series". In: *Revista Mexicana de Física* 52.2 (2006), pp. 155–162.

[10] J. S. Murguía et al. "Wavelet characterization of hyper-chaotic time series". In: *Revista Mexicana de Física* 64.3 (2018), pp. 283–290.

[11] L. P. Arts and E. L. Van den Broek. "The fast continuous wavelet transformation (fCWT) for real-time, high-quality, noise-resistant time–frequency analysis". In: *Nature Computational Science* 2.1 (2022), pp. 47–58. DOI: 10.1038/s43588-021-00183-z.

[12] T. Guo et al. "A review of wavelet analysis and its applications: Challenges and opportunities". In: *IEEE Access* 10 (2022), pp. 58869–58903. DOI: 10.1109/ACCESS.2022.3179517.

[13] A. Kumar et al. "Stationary wavelet transform based ECG signal denoising method". In: *ISA Transactions* 114 (2021), pp. 251–262. DOI: 10.1016/j.isatra.2020.12.029.

[14] C. Sidney, A. Ramesh, and H. Guo. *Introduction to Wavelets and Wavelet Transforms: A Primer*. Upper Saddle River, New Jersey: Prentice Hall, 1998.

[15] P. P. Vaidyanathan and I. Djokovic. "Wavelet transforms". In: *Mathematics for Circuits and Filters*. CRC Press, 2022, pp. 131–216.

[16] Stephane Georges Mallat. *Multiresolution representations and wavelets*. University of Pennsylvania, 1988.

[17] V. P. Koverda and V. N. Skokov. "Random process with a turbulent power spectrum". In: *Physica A: Statistical Mechanics and its Applications* 612 (2023), p. 128491. DOI: 10.1016/j.physa.2023.128491.

[18] Gregory W Wornell and Alan V Oppenheim. "Estimation of fractal signals from noisy measurements using wavelets". In: *IEEE Transactions on signal processing* 40.3 (2002), pp. 611–623.

[19] Darryl Veitch and Patrice Abry. "A wavelet-based joint estimator of the parameters of long-range dependence". In: *IEEE Transactions on Information Theory* 45.3 (2002), pp. 878–897.

[20] J. R. Pulido-Luna et al. "A two-directional grid multiscroll hidden attractor based on piecewise linear system and its application in pseudo-random bit generator". In: *Integration* 81 (2021), pp. 34–42. DOI: 10.1016/j.vlsi.2021.04.011.

[21] R. D. J. Escalante-Gonzlez and E. Campos. "Multistable Systems with Hidden and Self-Excited Scroll Attractors Generated via Piecewise Linear Systems". In: *Complexity* 2020.1 (2020), p. 7832489. DOI: 10.1155/2020/7832489.

[22] E. Campos-Cantn et al. "Multiscroll attractors by switching systems". In: *Chaos: An Interdisciplinary Journal of Nonlinear Science* 20.1 (2010). DOI: 10.1063/1.3314278.

[23] F. Li and J. Zeng. "Multi-scroll attractor and multi-stable dynamics of a three-dimensional jerk system". In: *Energies* 16.5 (2023), p. 2494. DOI: 10.3390/en16052494.

[24] Eduardo Jiménez-López et al. "Generalized multistable structure via chaotic synchronization and preservation of scrolls". In: *Journal of the Franklin Institute* 350.10 (2013), pp. 2853–2866.

[25] Amr Sayed Abdel Fattah et al. "Denoising algorithm for noisy chaotic signal by using wavelet transform: Comprehensive study". In: *2011 International Conference for Internet Technology and Secured Transactions*. IEEE. 2011, pp. 79–85.

[26] Ruoqiu Wang. *Self-similar based time series analysis and prediction*. University of Toronto (Canada), 2014.

[27] Amit Kumar and Mandeep Singh. "Optimal selection of wavelet function and decomposition level for removal of ECG signal artifacts". In: *Journal of Medical Imaging and Health Informatics* 5.1 (2015), pp. 138–146.

[28] Ingrid Daubechies. "The wavelet transform, time-frequency localization and signal analysis". In: *IEEE transactions on information theory* 36.5 (2002), pp. 961–1005.

[29] G. W. Wornell and A. V. Oppenheim. "Wavelet-based representations for a class of self-similar signals with application to fractal modulation". In: *IEEE Transactions on Information Theory* 38 (1992), pp. 785–800. DOI: 10.1109/18.119736.